ChemPlusChem

Research Article
doi.org/10.1002/cplu.202400159

Chemistry Europe
European Chemical Societies Publishing

www.chempluschem.org

Cation Dependence of Enniatin B/Membrane-Interactions Assessed Using Surface-Enhanced Infrared Absorption (SEIRA) Spectroscopy

Barbara Daiana Gonzalez,[a] Enrico Forbrig,[a] Guiyang Yao,[b] Patrycja Kielb,[c, d] Maria Andrea Mroginski,[a] Peter Hildebrandt,[a] and Jacek Kozuch*[e, f]

Enniatins are mycotoxins with well-known antibacterial, antifungal, antihelmintic and antiviral activity, which have recently come to attention as potential mitochondriotoxic anticancer agents. The cytotoxicity of enniatins is traced back to ionophoric properties, in which the cyclodepsipeptidic structure results in enniatin:cation-complexes of various stoichiometries proposed as membrane-active species. In this work, we employed a combination of surface-enhanced infrared absorption (SEIRA) spectroscopy, tethered bilayer lipid membranes (tBLMs) and density functional theory (DFT)-based computational spectroscopy to monitor the cation-dependence (M^{z+} = Na^+, K^+, Cs^+, Li^+, Mg^{2+}, Ca^{2+}) on the mechanism of enniatin B (EB) incorporation into membranes and identify the functionally relevant EB_n:M^{z+} complexes formed. We find that Na^+ promotes a cooperative incorporation, modelled via an autocatalytic mechanism and mediated by a distorted 2:1-EB_2:Na^+ complex. K^+ (and Cs^+) leads to a direct but less efficient insertion into membranes due to the adoption of "ideal" EB_2:K^+ sandwich complexes. In contrast, the presence of Li^+, Mg^{2+}, and Ca^{2+} causes a (partial) extraction of EB from the membrane via the formation of "belted" 1:1-EB:M^{z+} complexes, which screen the cationic charge less efficiently. Our results point to a relevance of the cation dependence for the transport into the malignant cells where the mitochondriotoxic anticancer activity is exerted.

Introduction

Enniatins are mycotoxins produced by pathogenic *Fusarium* fungi[1,2] and are commonly found contaminants of cereal grains, animal feeds, and food commodities.[3–5] Due to their remarkable resistance against heat, acid and digestion, they can propagate through food and feed chains. This group of molecules is therefore of increasing concern for human and animal health at chronic exposure.[6,7] However, at the same time, enniatins have come to attention as potential anticancer agents[8] due to their specific cytotoxic properties against malignant cells.[9–13] Enniatins are well known for their ionophoric behaviour by which they exert antibacterial, antifungal, antihelmintic and antiviral activity.[14,15] The same behaviour is considered to be responsible for the primary mechanism of toxicity against cancer cells, which disturbs the physiological homeostasis by transporting cations through cell membranes leading to apoptotic cell death.[3] Since enniatins can be conveniently derivatized using the concept of hybrid modular non-ribosomal peptide synthetases, they present a promising class of anticancer agents that need to be explored in terms of their detailed molecular mechanism of action.[16]

Enniatins are cyclohexadepsipeptides that are composed of an alternating structure of three hydrophobic N-methylated amino acids (such as valine, leucine or isoleucine) and three hydroxyl acids (typically hydroxyvaleric acid) forming a six-unit ring structure.[1,2] To date, approximately 29 variants have been found and further biosynthesized to investigate their biomedical applications, with the valine-containing enniatin B (EB) being one of the most prevalent, active and best studied example (Figure 1A). Due to the hydrophobicity of the side-chains, EB and other enniatins can incorporate into cell membranes, where – as demonstrated by electrophysiological experiments – they increase the transmembrane flux of mono- and divalent cations[15] similar to beauvericin and valinomycin.[17,18] Furthermore, it was found that EB has a

[a] B. D. Gonzalez, E. Forbrig, M. A. Mroginski, P. Hildebrandt
Institut für Chemie, Technische Universität Berlin, Sekr. PC14, Straße des 17. Juni 135, D-10623 Berlin, Germany

[b] G. Yao
Institut für Chemie, Technische Universität Berlin, Straße des 17. Juni 124, D-10623 Berlin, Germany

[c] P. Kielb
Clausius Institut für Physikalische und Theoretische Chemie, Universität Bonn, Wegelerstr. 12, D-53115Bonn, Germany

[d] P. Kielb
Transdisciplinary Research Area, Building Blocks of Matter and Fundamental Interactions (TRA Matter), Universität Bonn, D-53115 Bonn, Germany

[e] J. Kozuch
Fachbereich Physik, Freie Universität Berlin, Arnimallee 14, D-14195 Berlin, Germany

[f] J. Kozuch
Forschungsbau SupraFAB, Freie Universität Berlin, Altensteinstr. 23a, D-14195 Berlin, Germany
E-mail: jacek.kozuch@fu-berlin.de

Supporting information for this article is available on the WWW under https://doi.org/10.1002/cplu.202400159

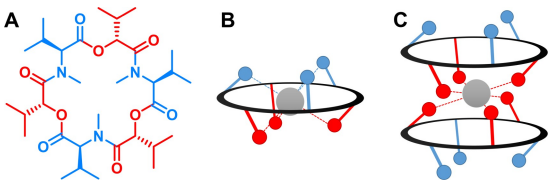

Figure 1. A: Chemical structure of enniatin B with hydroxyvaleric acid and L-valine units highlighted in red and blue, respectively. B, C: Schematic representations of $EB_n:M^{z+}$ 1:1 and 2:1 "sandwich" complex. The metal ion, amide and ester carbonyl oxygen atoms are depicted in grey, red and blue, respectively.

preference of mono- over divalent cations and a slightly pronounced specificity for K^+ over Na^+ ions according to the conductivity series $K^+ > Ca^{2+} \geq Na^+ > Mg^{2+} > Li^+$.[15] Interestingly, it has been suggested that this ion flux is accomplished by the existence of several distinct $EB_n:M^{z+}$ complexes in the lipid membrane with different stoichiometries.[14,19,20] Based on the possible coordination of cations via the three amide carbonyl groups and the three ester carbonyl groups several distorted octahedral $EB_n:M^{z+}$ complexes have been proposed: (a) a 1:1 complex where the metal ion is positioned in the middle of the EB ring (Figure 1B), (b) a "sandwich" 2:1 complex with the metal cation between two EB rings (Figure 1C), and (c) a much less likely "double-sandwich" 3:2 complex in which one EB ring is located between two metal ions that are enclosed by two EBs. While in the 1:1 complex all carbonyls of one EB molecule are involved in coordination, in 2:1 and 3:2 complexes either amides or esters (all amide and ester carbonyls are pointing towards opposite sides of the ring, see Figure 1) can contribute to coordination. It was discussed previously that amide carbonyls are preferable ligands, so that, e.g., amide-amide-coordinated 2:1 complexes are predominant, which, in principle, makes the existence of 3:2 complexes in general less likely.[20] Experimental studies of these potential complexes in organic solvents supported such a situation while crystallography of an admixture of EB and K^+SCN^- suggests in general that both coordinations (ester and amide) are viable in a crystal.[14,19–21] However, even though these studies provided initial knowledge on the structure of $EB_n:M^{z+}$ complexes in various environments, much knowledge is missing regarding EB's cation-dependent mechanism of incorporation and its structure-function relationship in lipid membranes, where it exerts its natural bioactive function. This understanding is essential to guide the design of more active derivatives.

In order to address this question, we combine tethered bilayer lipid membranes (tBLMs)[22] on Au supports with surface-enhanced infrared absorption (SEIRA) spectroscopy,[23] which was demonstrated to provide insight into the structure, orientation and function of membrane proteins[24–31] and membrane-active (antimicrobial) peptides.[32–36] The particular strength of this approach lies in the plasmonic enhancement of IR signals of molecules in close vicinity to the nanostructured Au support (up to ca. 8 nm), which allows selectively detecting processes occurring at the membrane interface or inside the membrane without the interference from the bulk,[23] while changing the ion composition or pH.[27,32,37]

In this work, we employed the tBLM-SEIRA approach, complemented by density functional theory (DFT), to characterize the effect of different cations on the mechanism of EB incorporation into membranes and provide insight into the structure and nature of EB:cation complexes that are responsible for its ionophore function using calculations. We show that presence of Na^+ leads to a positive cooperative process of incorporation, while interaction with K^+ leads to a direct but less efficient insertion into membranes. Furthermore, whereas our SEIRA data shows that membrane-incorporated EB can exchange Na^+, K^+ and Cs^+ reversibly, the cyclodepsipeptide is (partially) extracted from the membrane by ions according to the series $Ca^{2+} < Mg^{2+} < Li^+$, providing a rationale for the observed conductivity series. Finally, via comparison of SEIRA and DFT-based spectra we provide an assignment to different EB:cation complexes that, in select cases, contradict those from experiments in organic solvents.

Methods and Materials

Materials

6-Mercaptohexanol (6MH, Sigma-Aldrich), 1-palmitoyl-2-oleyl-sn-glycero-3-phosphocholine (POPC, Avanti Polar Lipids), bis-tris propane (BTP), lithium chloride, sodium chloride, potassium chloride, magnesium chloride, calcium chloride, sodium tetrachloroaurate(III) trihydrate (all Sigma-Aldrich), and ceasium chloride (Merck) were purchased at highest purity grade available. WK3SH [(β-cholestanoxy)ethoxy)ethoxy)ethanethiol] was synthesized as described previously.[25] Enniatin B (EB) was synthesized according to previous work.[38] Buffer solutions were prepared using Milli-Q-water with a resistance of $>18\ M\Omega cm$ and were based on 20 mM BTP and 100 mM MCl_n at pH 7.4 (with M = Li, Na, K, Cs, Mg, Ca).

Surface-Enhanced Infrared Absorption Spectroscopy

All spectroscopic experiments were performed using a Bruker IFS66v/s spectrometer equipped with a MCT photoconductive detector and a Kretschmann-ATR setup adjusted to an angle of incidence of 60°. For each spectrum, 400 scans were acquired in the spectral range of 4000 to 1000 cm^{-1} and at a spectral resolution of 4 cm^{-1}. Nanostructured Au films for SEIRA spectroscopy were produced by electroless deposition from an a $NaAuCl_4$ solution according to Miyake et al.[39]

Tethered Bilayer Lipid Membrane Construction and Incorporation of Enniatin B

The nanostructured Au film was functionalized with a mixed self-assembled monolayer (SAM) of WK3SH and 6MH, which was incubated overnight in a solution of 0.6 mM WK3SH and 0.4 mM 6MH in 1-propanol. Evaluating the capacitance indicated a WK3SH:6MH ratio of ~70:30 (1.3–1.5 $\mu F/cm^2$ – see Figure S1 and SI section 1 for more details) on the electrode surface as required for the formation of tBLMs with 6MH-supported free standing BLM domains.[25,32,40,41] Unilamellar POPC vesicles were prepared according to Schmitt et al. at a final concentration of 0.5 $mg\,mL^{-1}$ by extrusion through polycarbonate filters with a pore size of 200 nm in 100 mM NaCl and 20 mM BTP buffer at pH 7.4.[42] The tBLM was assembled by addition of the unilamellar vesicles onto the SAM.

After two to three hours, the suspension was replaced by a vesicle-free buffer solution. The formation of the tBLM was confirmed in each experiment by recording SEIRA spectra as well as the capacitance and resistance of the membrane as shown previously (capacitance of well formed tBLM was around 0.9 μF/cm^2, see Figure S1).[25,32–34,40] Ethanol-dissolved EB was added to the supernatant buffer solution at a concentration of 100 μM such that the ethanol solution did not exceed 2%; the integrity of the membrane was maintained as assessed via capacitance measurements (Figure S1).

Calculations of Computational Infrared Spectra

Geometry optimization and vibrational analysis using normal mode analysis of the $EB_n{:}M^{z+}$ complexes was performed with the functional BP86[43,44] in Gaussian16.[45] Based on related studies on complexes of (alkali) metals and organic molecules,[46,47] C, N, O and H atoms were treated using the 6–31 g* basis set,[48] and the alkaline and alkaline earth metal ions were described using def2-TZVP basis set[49] together with its core potential[50] for Cs^+. In addition n-pentadecane was specified as solvent in a polarizable continuum model to mimic the hydrophobic parts of the membrane.[51] Initial structures were based on crystal structures of belted 1:1 and 2:1 sandwich complexes with Na^+ and K^+ from previous studies (QQQGMD and IHECUT in the Cambridge Structure Databank[52]).[21,53] Infrared spectra were determined through normal mode analysis and are displayed without corrections using scaling factors; ester and amide C=O stretching modes are shown using a band width (FWHM) of 8 and 16 cm^{-1} to match the experimental spectral shapes. Optimized structures are deposited under https://github.com/KozuchLab/Publications/tree/main/Enniatin_DFT.

Results

Cation-Dependent Incorporation of EB Into tBLMs.

Incorporation of EB into cellular membranes represents the basis for its action as an ionophore. Since Na^+ and K^+ are the most prevalent cations in the extracellular medium[54] and K^+ is the cation that EB has the highest selectivity towards,[15] we studied their influence on the EB incorporation mechanism. To analyse the effect, we constructed tBLMs using POPC as lipid. These model membranes were assembled on a phase-separated mixed self-assembled monolayer (SAM) composed of 6-mercaptohexanol and the cholestanol-tethered WK3SH, and characterized using SEIRA and electrochemical impedance spectroscopy, similar to our previous studies (Figure S1).[25,33,34] EB was added at a concentration of 100 μM into the supernatant solution containing 100 mM of Na^+/K^+ that covered the tBLM. SEIRA spectra were recorded taking the spectrum of the tBLM with the same ions as reference. Due to the distance-dependent decay of the enhancement in SEIRA (decaying with d^{-6}),[55] bulk water does not or only weakly interferes with the spectrum. Therefore, almost exclusively spectral changes originating from EB (or lipids) are observed in the SEIRA spectrum in the 1850–1500 cm^{-1} region. In certain cases, these spectral features may overlap with minor changes of water molecules at the membrane/solution interface occurring at ca. 1650 cm^{-1} (H_2O bending mode). The correction of such an overlap is straightforward due to the broad width of this spectral feature compared to the much narrower bands of EB and lipids, and the intense H_2O stretching modes at ca. 3400 cm^{-1} (Figure S2).[33]

Figure 2A shows SEIRA spectra monitoring the incorporation of EB into the tBLM in the presence of Na^+ or K^+. In both cases, two bands are observed that can be readily assigned to the C=O stretching modes of the esters and amides (spectral position denoted as $\nu(CO_{ester})/\nu(CO_{amide})$ in the following), i.e. at 1746/1659 cm^{-1} for Na^+ and 1747/1665 cm^{-1} for K^+ (see DFT section below), showing evidence for association of EB with the membrane. In contrast to other "regular" peptides, in which amide I and amide II modes are characteristic marker bands in the IR spectrum,[33,34,56,57] EB does not have an amide II mode (~1550 cm^{-1}) due to the methylation of the amide nitrogen (Figure 1A). The differences in the exact positions of these modes will be discussed later in this work. A major contribution of lipid C=O modes (at ca. 1735 cm^{-1}) to the EB ester mode can be excluded based on the narrow width of the EB-ester mode.[25,27,32] Further CH_n modes of lipids are found in the range 3000–2900 cm^{-1} and are used to infer changes to the lipid membrane.[58,59] Changes to these modes are small in our experiments (Figure S2 and S3) suggesting that EB incorporation does not affect the lipid integrity. A detailed analysis of this spectral region is not performed herein, due considerable overlap with EB's CH_n modes requiring isotope labelling for a clear deconvolution. In addition to the experiments in presence of Na^+ and K^+, we repeated this experiment in the absence of any ions, i.e. with water as supernatant solvent, but did not detect any spectral features specific to EB (Figure S3).

The time evolution of both ester and amide signals during EB incorporation is shown in Figure 2B, C. Comparing both traces one can observe major differences between EB's behaviour with Na^+ and K^+. Accordingly, after an initial burst of binding that decays rapidly, a plateau is reached immediately or develops gradually in the presence of Na^+ or K^+, respectively. However, after ca. 30 min only in presence of Na^+ an unexpected and pronounced sigmoidal increase occurs, which provides evidence for a distinctly different mechanism of EB incorporation. After a constant amide intensity was reached at ca. 1.3 mOD and 0.7 mOD (or $60\cdot10^{-3}$ and $25\cdot10^{-3}$ according to integrated intensity as shown in Figure 2B, C) with Na^+ and K^+, respectively, the buffer was replaced to remove residual EB in the bulk, which led to a decrease of the EB signals to roughly 65% of the intensity before the wash in both cases. This observation indicates a substantial amount of surface-bound EB on the membrane interface during incubation. At the same time, the washing step leads to slight changes of both bands in presence of Na^+, where the $\nu(CO_{amide})$ shifts from 1659 cm^{-1} to 1658 cm^{-1} as appreciable more clearly in the difference spectra (grey spectra; after scaling to similar absolute intensities). Since the amide C=O groups are more likely to coordinate the ions, this shift indicates the existence of a mixture of different $EB_n{:}Na^+$ species when covering or incorporated into the membrane. In the case of K^+ no changes are observed to the amide band, indicating only one species or a mixture of species with maintained composition. Less pronounced changes are detectable only for the ester mode with both ions. The difference band centered around 1740 cm^{-1} can be assigned

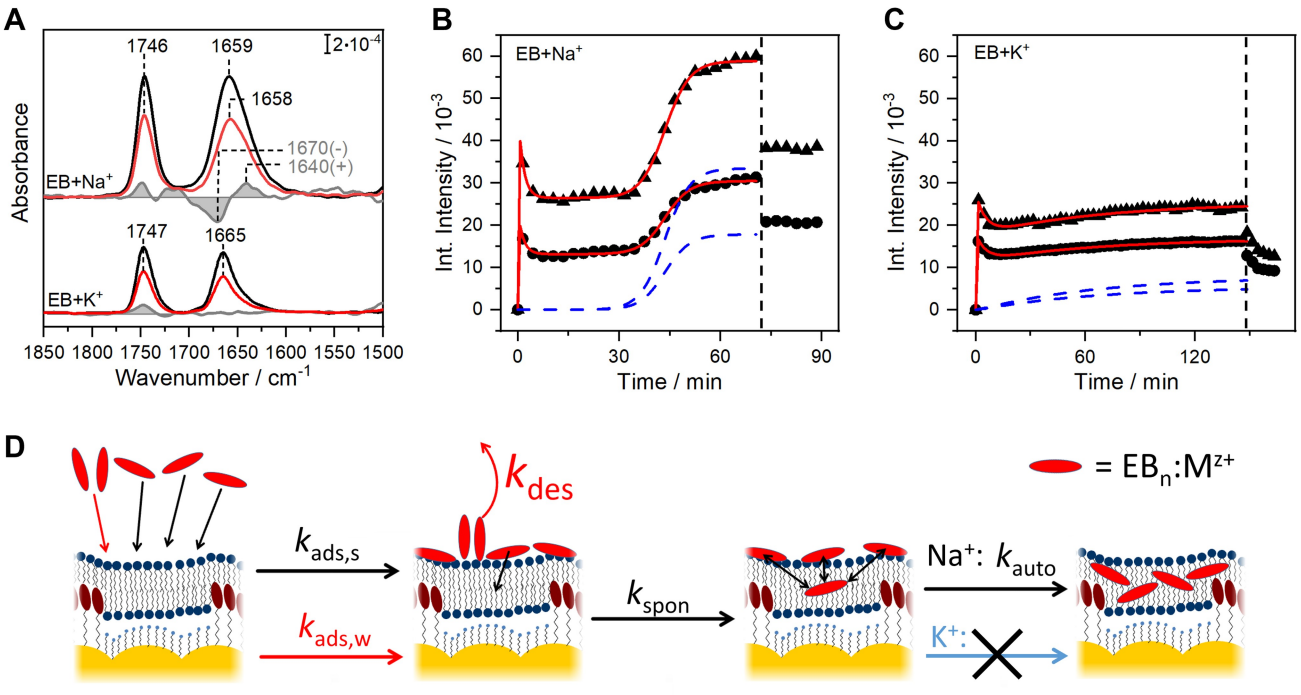

Figure 2. A: SEIRA spectra of EB incorporation in presence of Na^+ (top) and K^+ (bottom). Spectra of completed incubation (when plateau is reached) and after buffer exchange to remove excess EB are shown in black and red, respectively. Grey spectra are scaled difference spectra ("red-minus-black") where both red and black are scaled to approximately similar intensity and are enhanced by a factor of 4 for clarity. **B, C**: Time traces of integrated intensities of ester (~1745 cm^{-1} in A; triangles) and amide C=O stretches (~1660 cm^{-1} in A; circles) in the presence of Na^+ (**B**) and K^+ (**C**); wash with new buffer solution is indicated by dashed line. Red lines are results from modelling the time traces with the kinetic model in **D**; blue dashed lines represent the fraction of EB, which was incorporated into the membrane core, i.e. the last two states in **D**. **D**: Kinetic model to describe the data in presence of Na^+ (**B**; see main text and SI section 5 for details); red ellipses represent EB molecules as part of $EB_n:M^{z+}$-complexes. Initially EB molecules adsorb onto the membrane interface weakly ($k_{ads,w}$; this fraction desorbs then with k_{des}) or strongly ($k_{ads,s}$), leading to the initial burst. The adsorbed species either enter the membrane spontaneously (k_{spon}) or autocatalytically (k_{auto}) by the presence of already inserted EB molecules. The data in presence of K^+ (**C**) were modelled with a truncated version, i.e. without the autocatalytic incorporation step. Data for EB incorporation in the presence of Cs^+ and in the absence of any ions are shown in Figure S3. Note that EB complexes may adopt a range of orientation and not only the ones shown as examples in this figure.

either to minor changes of the lipid's C=O stretches or can originate directly from solvatochromic shift (hydrophobic membrane core vs. polar head groups)[60,61] of EB's $\nu(CO_{ester})$ modes upon removal of solvent exposed EB:K^+ complexes. Incorporation in the presence of Cs^+ showed a similar behaviour to K^+ and is discussed in the SI (Figure S3).

Effect of Cation Exchange on Membrane-Bound EB

To analyse the structural changes of EB involved in conductance of different cations, we continued with a tBLM system in which EB was incorporated in the presence of Na^+ (after at least 1 h of incorporation) and exchanged ions to K^+, Cs^+, Li^+, Mg^{2+} and Ca^{2+} (Figure 3A). Ion exchange with Na^+, K^+ and Cs^+ showed a reversible behaviour (Figure S4), as apparent by an approximately constant (or increased) SEIRA intensity, so that these experiments were performed on the same tBLM. However, Li^+, Mg^{2+} and Ca^{2+} showed irreversible changes (Figure S4) that decreased the absorbance of EB and led to much less defined spectral features than in Na^+, K^+ and Cs^+ (see enlarged spectra in Figure 3B). As a consequence, ion exchange to Li^+, Mg^{2+} and Ca^{2+} was performed on separate membrane systems. EB + Na^+ and EB + K^+ SEIRA spectra from ion exchange experiments show same peak positions (1746/1658 cm^{-1} and 1747/1665 cm^{-1}, respectively) and line shapes as during the incorporation (Figure 2A) pointing to a completed replacement of these ions in $EB_n:M^+$ complexes in the membrane (the same is true for Cs^+, see Figure S3). At the same time, the absolute SEIRA intensities are inverted. EB incorporation in presence of K^+ led to 3 times lower intensities than in Na^+, whereas here exchange of ions from Na^+ to K^+ induces an increase in absorbance by 1.4 of both $\nu(CO_{ester})$ and $\nu(CO_{amide})$ modes. This effect can be ascribed primarily to an increasing surface enhancement of the IR signal with proximity to the SEIRA Au surface, and as such to a relocation of EB towards the electrode-facing side of the tBLM, or possibly to a more favourable orientation of the ester and amide C=O groups with the surface selection rule.[27,33,34] A change of number of EB molecules at/in the membrane can be excluded due to reversibility when ions are exchanged. Interestingly, this change of intensity is in line with the previously reported preference of binding K^+ over Na^+ by a factor of 1.4 and thus may directly reflect the extent of binding (note that the similarity of both numbers is coincidental).[15] Exchange to Cs^+ only leads to minor changes in frequency (1746/1659 cm^{-1}), more clearly

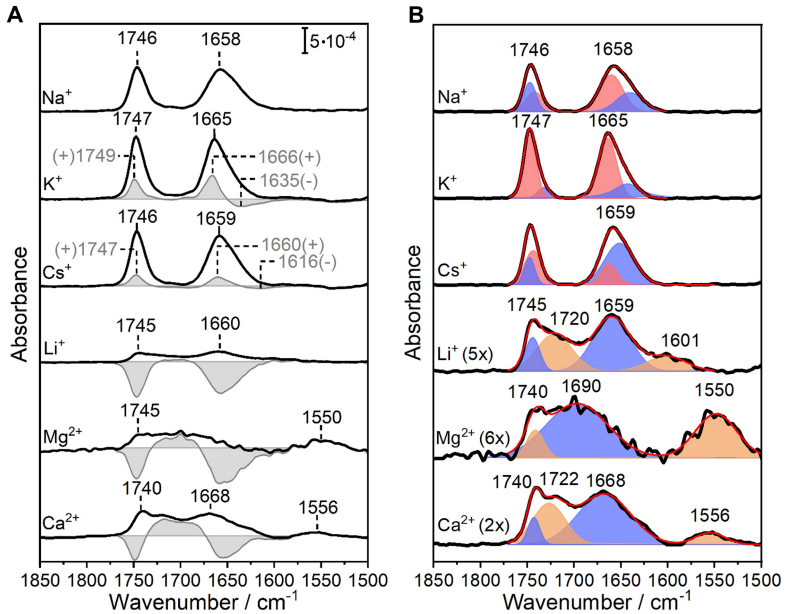

Figure 3. SEIRA spectra of membrane-incorporated EB after buffer exchange from Na^+ to K^+, Cs^+, Li^+, Mg^{2+}, and Ca^{2+} (from top to bottom in both **A** and **B**). **A**: Black lines show spectra after ion exchange; grey filled spectra represent the difference spectra vs. the spectrum in presence of Na^+. Exchange between Na^+, K^+, and Cs^+ was reversible, such that spectra from a single experiment are depicted (see Figure S4). Due to irreversible behavior in Li^+, Mg^{2+}, and Ca^{2+}, spectra were obtained from individual experiments and are scaled such that the spectrum in Na^+ prior to buffer exchange had similar intensities. **B**: Peak fit to spectra in **A** with red lines showing the overall fits, and red, blue and orange filled features depicting band shapes (red, blue and yellow peaks are assigned via comparison to DFT-based spectra to the species shown in Figure 4).

demonstrated in the difference spectrum, and increases intensity by 1.2 in comparison to the spectrum in presence of Na^+. The associated spectral changes are more clearly visible in the difference spectra when exchanging from Na^+ to K^+ or Cs^+, where the difference peak of the amide mode displays a positive lobe at slightly higher frequencies of 1666 or 1660 cm^{-1}, respectively. The $\nu(CO_{ester})$ shows a slight blueshift and an increase in intensity. Previously, Ovchinnikov et al. have determined IR spectra of $EB_n{:}M^+$ complexes to identify specific complexes in acetonitrile as solvent.[14] Surprisingly, in their work IR spectra of EB with Na^+, K^+ and Cs^+ did not show any considerable difference (1746–1744/1666–1665 cm^{-1}) while the very similar beauvericin (with phenylalanine instead of valine) displayed much more significant changes. Apart from a solvatochromic effect due to different environments, it is obvious that EB behaves differently when incorporated into a membrane than in an organic solvent, so that the structural assignment to complexes of different stoichiometry must be revisited.

In contrast, exposure to Li^+, Mg^{2+} or Ca^{2+} decreased the spectral intensity considerably (by factors of 5, 3 or 1.7, respectively) and yielded broadened spectra with less defined peaks. The irreversibility of the change in absorbance (Figure S4) points to cation-induced removal of EB from the membrane core towards the membrane/bulk interface or even into the bulk solution. These scenarios are further supported by the difference spectra upon ion exchange, in which the negative peaks resemble lost signal of the spectral shapes observed in Na^+. As such, we observe the lowest intensities of EB absorption peaks for Li^+, and the least defined spectrum with weakly identifiable peaks in the presence of Mg^{2+}. For Li^+ and Ca^{2+} peaks are identified at ca. 1745/(1720)/1659 cm^{-1} and 1740/(1722)/1668 cm^{-1}, while the position of the "middle" peak may be inaccurate due its weak intensity and broad background. With the bivalent Mg^{2+} and Ca^{2+} an additional broad band at 1550–1560 cm^{-1} is observed, which is not present with monovalent cations.

To assess if and how many components are contributing to the spectra, we modelled the spectra using Gaussian band shapes (Figure 3B). As obvious from the asymmetric band shapes in Na^+, K^+, and Cs^+, two components were necessary for a satisfactory fit to the spectra. However, while in K^+ the red components were clearly dominating both $\nu(CO_{ester})$ and $\nu(CO_{amide})$ bands, in Na^+ and Cs^+ a ratio of between approx. 2:1 to 1:2 is adopted between band indicated in blue and red. This suggests that K^+ shows a pronounced preference for a single $EB_n{:}M^{z+}$ species, whereas for Na^+ and Cs^+ a mixture of approximately equally prevalent complexes occurs. The latter appears to be also the case in Li^+, Mg^{2+} or Ca^{2+} with several strongly overlapping bands.

Density Functional Theory Calculation of Various $EB_n{:}M^{z+}$ Species

DFT calculations and normal mode analysis have been performed for a series of possible $EB_n{:}M^{z+}$ complexes with different stoichiometries and free EB in a polarizable continuum model (PCM) of n-pentadecane. The choice of PCM was to imitate the environment of the hydrophobic membrane in

comparison to the SEIRA spectra. In principle one can imagine that $EB_n:M^{z+}$ complexes can preferably reside either in the membrane core or in the lipid head group region. However, the anisotropy of the dielectric constant of the head group region and the complexity of direct intermolecular interactions do not permit a straightforward and reliable prediction of such environments using DFT. In order to facilitate the comparison to the SEIRA spectra, simulated IR spectra are shown using Gaussian band shapes and FWHM values of 8 cm^{-1} and 16 cm^{-1} for $\nu(CO_{ester})$ and $\nu(CO_{amide})$ modes, respectively, similar to the experimental IR bands. For each cation three different structural models have been simulated (Figure 4): (a) a $EB:M^{z+}$-1:1 belted complex (yellow) and (b) a $EB_2:M^{z+}$-2:1 sandwich complex (red), both shown schematically in Figure 1, as well as (c) a $EB:M^{z+}$-1:1 open-faced sandwich complex (blue), where one EB molecule is removed from a 2:1 complex. These structures will be referred to as $EB:M^{z+}{}_{in}$, $EB_2:M^{z+}$, and $EB:M^{z+}{}_{out}$, respectively, in the following. The open-faced sandwich structure $EB:M^{z+}{}_{out}$ is a probable intermediate in the formation of $EB_2:M^{z+}$ complexes or in cation release from both $EB_2:M^{z+}$ and $EB:M^{z+}{}_{in}$ complexes and therefore may be observed in the SEIRA spectra. We are aware that in such an open-faced structure the cation will be ligated from the open face by either water molecules, anions or carbonyls or phosphate groups of lipids (or a combination of those) and consequently will reside at the membrane core/headgroup interface. If present, a mixture of these species will be detected using SEIRA, but it is not feasible to model the entire distribution of possible ligations using DFT for a comparison with experimental spectra. Thus we only simulated ligand-free $EB:M^{z+}{}_{out}$ structures in each case as a representative of these structures.

A successful structural optimization was not achieved in each EB-cation combination and complex (Figure 4 right). Accordingly, the "ideal" 1:1 $EB:M^{z+}{}_{in}$ complex as depicted in Figure 1 was only stable with Na^+, Mg^{2+} and Ca^{2+}, where the ions were coordinated by all six oxygen atoms of esters and amide, with the ion lifted slightly towards the amide groups. With Li^+ instead a highly distorted structure was obtained, where the small ion experiences a pseudo-tetrahedral coordination by two amide and two ester groups. However, with K^+ and Cs^+, this structure was unstable and the cation was released out of the EB ring to afford a stable amide-ligated $EB:M^{z+}{}_{out}$ structure suggesting that 1:1 belted $EB:M^{z+}{}_{in}$ complexes of these two cations do not exist. The open-faced $EB:M^{z+}{}_{out}$ structure was stable with all tested ions. The $EB_2:M^{z+}$ sandwich complex, as shown in Figure 1 and demonstrated or proposed previously, was obtained with K^+, Cs^+, Mg^{2+} and Ca^{2+}. Instead, with Na^+ and Li^+ distorted structure was formed. Na^+ was still coordinated by three amides of one EB ring, but the second ring "lifted off" and added only two additional amide coordinations creating a displaced EB-EB arrangement. With Li^+ the distortion was even more pronounced, where a trigonal coordination was achieved by two amides from one and the third from the other EB ring.

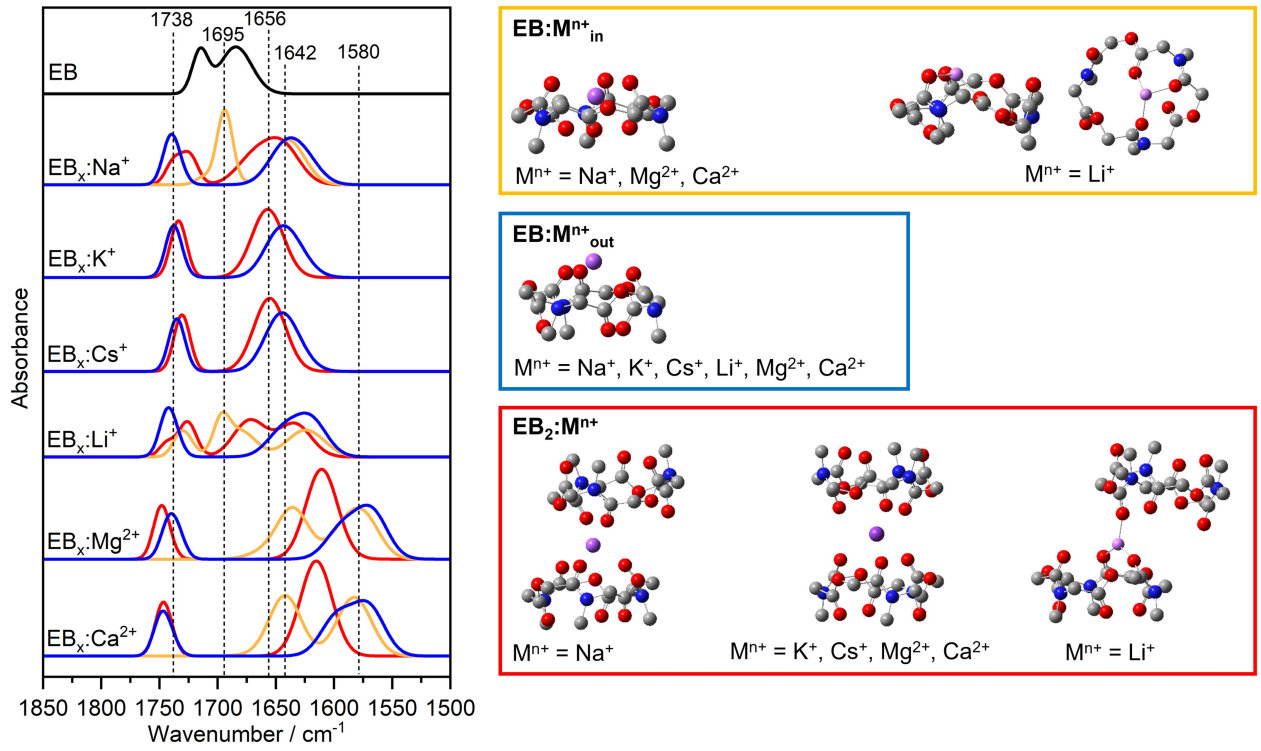

Figure 4. Left: DFT-based computational IR spectra of $EB_n:M^{z+}$ complexes: $EB:M^{z+}{}_{in}$ in yellow, $EB:M^{z+}{}_{out}$ in blue, and $EB_2:M^{z+}$ in red with ion used in the experiments; the black spectrum (top) is EB without ions. Labels and dashed lines indicate approximate positions of peaks in the DFT-based IR spectra and are shown to ease the comparison of spectra with different ions. **Right**: Representative structures obtained after optimization using DFT. $EB:M^{z+}{}_{in}$ (yellow) is obtained with Na^+, Mg^{2+}, and Ca^{2+}, but not with K^+ and Cs^+; with Li^+ a distorted structure is adapted. $EB:M^{z+}{}_{out}$ (blue) is obtained with all tested ions. $EB_2:M^{z+}$ (red) converges with K^+, Cs^+, Mg^{2+}, and Ca^{2+}; with Na^+ and Li^+ distorted structures are formed. Hydrogen atoms and iso-propyl groups are not shown for clarity.

These ion-dependent and diverse structures have consequences on the IR spectra computed via normal mode analysis (Figure 4 left). Overall, simulated IR spectra support the previous assignment of the high-frequency and low-frequency bands in the 1750–1600 cm^{-1} region to the ester (~1738 cm^{-1}) and amide carbonyl stretches (1660–1640 cm^{-1}), respectively, in presence of Na^+, K^+ and Cs^+. For C_3-symmetric structures, these bands are dominated by the symmetric mode and a non-appreciable contribution of the anti-symmetric modes occurring as redshifted shoulders (by ca. 6 cm^{-1}). Non-coordinating ester carbonyls are predicted to absorb in the range around 1738 cm^{-1} for $EB_2:M^{z+}$ and $EB:M^{z+}{}_{out}$ open-faced complexes. In $EB:M^{z+}{}_{in}$ complexes the ester groups contribute to complexation and are thus shifted to ca. 1695 cm^{-1} for Na^+ and Li^+, which can be used as a specific marker for the $EB:M^{z+}{}_{in}$ complex with monovalent cations. The coordinating $\nu(CO_{amide})$ is located at 1660–1625 cm^{-1}. In cases where the amide does not coordinate to the metal, it is predicted to absorb closer to 1680 cm^{-1}. With bivalent cations the ligating ester and amide groups are significantly redshifted to roughly 1640 and 1580 cm^{-1}, respectively, as a consequence of the high charge density of the metal ions.

Comparing the vibrational frequencies within the monovalent series for the open-faced $EB:M^{x+}{}_{out}$ structure (Figure 4 blue spectra and box), which in all cases let to a C_3-symmetric conformations, provides insight into the cation-dependent trends within one type of complex. Accordingly, the $\nu(CO_{ester})$ frequency is predicted to vary according to the series $Ca^{2+} > Li^+ > Mg^{2+} > Na^+ > K^+ > Cs^+$ by about 10 cm^{-1}. These predictions are overall in line with expectations from the vibrational Stark effect[62] when taking into account the out-facing orientation of the ester carbonyls, and the changing charge density of the ions. For the amide stretch we note the inverted trend of $Cs^+ \geq K^+ \geq Na^+ \geq Li^+ \gg Mg^{2+} \approx Ca^{2+}$ over almost 100 cm^{-1}, where one can expect that additional electronic polarization of the amides play a considerable role in addition to the vibrational Stark effect.[60,61] Importantly, the simulated spectra show that within similar types of complexes (see $EB_2:M^{z+}$ - red spectra; and $EB:M^{z+}{}_{out}$ - blue spectra) peak positions with K^+ and Cs^+ differ by only ± 1 cm^{-1} and are therefore not easily distinguished; this is also the case comparing Mg^{2+} and Ca^{2+}. Instead, in the $EB:M^{z+}{}_{out}$ (blue spectrum) with Na^+ the ester and amide C=O band are shifted by $+1$ cm^{-1} and -4 cm^{-1}, respectively, relative to K^+; with Li^+ this shift is more pronounced to $+3$ and -16 cm^{-1}, and with Mg^{2+}/Ca^{2+} to $+8$ and -82 cm^{-1}. Finally, non-ligating EB gives a very distinctive spectrum, which is easily distinguished from most EB:ion complexes by closely positioned ester and amide bands at 1715/1685 cm^{-1}. This information gives valuable guidelines for the analysis of the recorded spectra.

Discussion

Kinetics of Membrane Incorporation in the Presence of Na^+ or K^+

Sigmoidal trends have been often observed in concentration-dependent plots and indicate a positive cooperative behaviour, i.e. an increased activity or interaction at higher concentrations of a substrate. In enzymatic catalysis, for instance, this indicates allosteric effects in which binding of a ligand to an allosteric site increases the binding affinity and/or enzymatic activity towards its substrate.[63,64] Similarly, positive cooperativity in adsorption isotherms relate to an increased binding in proximity to other adsorbates.[65] In the present case, an analogous situation is conceivable where already membrane-incorporated EB molecules or $EB_n:M^{z+}$ complexes, in the presence of Na^+, support further integration in an *autocatalytic* fashion. Accordingly, due to the observed time delay of ca. 30 min, "regular" or spontaneous incorporation must be associated with a substantial barrier. To describe the entire incorporation behaviour, we translated a kinetic model to a differential equation system accounting for the following key processes (Figure 2D; for detailed description of this model see SI section 5). First, EB binds from the bulk to the membrane surface according to a Langmuir-like adsorption process. To account for the initial burst, two binding modes are assumed, i.e. strongly bound species, which do not show any considerable desorption, and weakly bound ones, which desorb from the membrane interface. Second, the strongly surface-bound species can transfer into the membrane via two mechanisms: (a) a spontaneous Langmuir-like incorporation according to

$$\frac{d[EB_{mem}]}{dt} = k_{spon} \cdot [EB_{ads}] \cdot (1-\theta) \quad (1)$$

and/or (b) an *autocatalytic* incorporation following the Prout-Tompkins model[66,67]

$$\frac{d[EB_{mem}]}{dt} = k_{auto} \cdot [EB_{ads}] \cdot [EB_{mem}] \cdot (1-\theta) \quad (2)$$

where k_{spon} and k_{auto} are the rate constants for spontaneous or autocatalytic incorporation, $[EB_{ads}]$ and $[EB_{mem}]$ the concentrations of complexes on the membrane surface or inside the membrane (here SEIRA intensities are used directly as a proxy for the concentrations), respectively, and θ the percentage of occupied space in the membrane. Despite the ability of monitoring and even quantifying orientational changes using SEIRA, due to the surface selection rule,[23,27,33] in this kinetic model we do not consider any reorientational processes explicitly. We assume implicitly that in each of the states of the model (Figure 2D) a specific but constant orientation distribution of EB species is adopted and remains unchanged.

The kinetic model was used to fit the traces of $\nu(CO_{ester})$ and $\nu(CO_{amide})$ intensities simultaneously (Figure 2B,C) and demonstrates a very good description of the sigmoidal evolution of EB intensity in presence of Na^+. At the same time, the truncated

version of this model, i.e. neglecting the autocatalytic process, can be used to provide a very good fit for the experiments in K^+ buffer showing that spontaneous incorporation is sufficient in this case (the same is the case in Cs^+, Figure S3). Using this model, we can directly compare the evolution of only the membrane-incorporated component (blue dashed lines) in presence of each ion. Accordingly, we note that interaction of EB with Na^+ leads to a considerably delayed incorporation than with K^+, but exceeds in level of incorporation by a factor of ca. 4 judging solely based on SEIRA intensity. Furthermore, this model and the fitting results are in line with the loss of intensity after wash with new buffer, which removes surface-bound EB at the membrane interface and leads to a decrease of intensities towards the level of incorporated EB according to the kinetic model (blue dashed lines).

It is now interesting to compare the effective rate constants of the spontaneous incorporation of EB with both ions. Accordingly, for Na^+ a k_{spon} value of $2 \cdot 10^{-7}\,min^{-1}$ is obtained which is smaller by 4 orders of magnitude than the one determined for K^+ of $2.5 \cdot 10^{-3}\,min^{-1}$. For the sake of comparison: if one assumes similar molecular mechanisms (and all other parameters being equal), this difference of the rate constants would translate to a drastically higher *effective* activation barrier of EB incorporation in presence of Na^+ ions by ca. 23.5 kJ/mol according to

$$\Delta G^{\ddagger}_{spon,Na} - \Delta G^{\ddagger}_{spon,K} = RT \cdot ln\left(\frac{k_{spon,Na}}{k_{spon,K}}\right) \quad (3)$$

where $\Delta G^{\ddagger}_{spon,i}$ are the activation barriers, R is the gas constant, and T the temperature. Such a pronounced difference points to the presence of distinctly different EB:cation species responsible for incorporation. These species shield the cationic charge of K^+ very efficiently, but fail to do so for Na^+.

Nature of $EB_n:M^{z+}$ Species in the Presence of Specific Cations

Ovchinnikov et al. showed that K^+ binds EB as $EB_2:K^+$ sandwich complexes in organic solvents.[14] Based on these results it was suggested that Na^+ and Ca^{2+} adopt similar structures, as similar peak positions of 1746–1744/1666–1665 cm^{-1} were observed with the ions for the $\nu(CO_{ester})/\nu(CO_{amide})$ modes. Comparing these previous FT-IR results obtained from acetonitrile solutions with the present SEIRA spectra of EB in tBLMs, we note similar peak positions of 1744/1666 cm^{-1} in presence of K^+, but not for Na^+ and Ca^{2+}. As discussed above and previously,[20] amide carbonyls are thermodynamically preferred ligands, so that in a 2:1 stoichiometry their vibrational frequency is highly sensitive to the carbonyl-metal interaction, while the ester CO modes report on the long-range electrostatics originating from the metal ion and the local electrostatics due to solvation, according to the vibrational Stark effect.[60,61] In this way, for K^+, a similar ligation pattern in acetonitrile and in tBLMs can be deduced from the match of amide frequency, whereas the 3 cm^{-1} difference of the ester vibration can be rationalized based on a solvatochromic blue-shift due to the more polar environment of acetonitrile in contrast to the membrane core.[60] As such, we can assign the major species observed in tBLMs in presence of K^+ to a membrane-incorporated $EB_2:K^+$ sandwich complex (see summarizing Figure 5). This is consistent with our DFT-based spectra, in which the $EB_2:K^+$ showed the most blue-shifted peak position (amide mode at 1656 cm^{-1}) of all complexes – the remaining 10 cm^{-1} offset between experiments and DFT is acceptable taking into account the level of theory used herein. Our assignment is further consistent with SEIRA signals of EB in presence of K^+ showed band shapes that were modelled with one dominating Gaussian peak (red peaks in Figure 3B). Consequently, the additional minor peaks (blue peaks in Figure 3B) can be assigned to small contributions of $EB:K^+_{out}$ residing at the membrane interface (Figure 5).

The discrepancies between our SEIRA data and previous results of EB-cation complexes in acetonitrile in presence of Na^+ and Cs^+ (i.e. the frequencies of amide modes at 1658 and 1659 cm^{-1} vs. 1665 and 1666 cm^{-1} in our results vs. those of Ovchinnikov,[14] respectively) indicate different species being adopted in membranes compared to the $EB_2:M^+$ as proposed in acetonitrile. We aim to assign the species observed in our SEIRA spectra by comparison to the set of spectra obtained using DFT. First, we can exclude the presence of $EB:Na^+_{in}$ (despite being proposed previously)[3] or free EB in our SEIRA spectra in Na^+, based on the absence of noticeable signals between the dominant $\nu(CO_{ester})$ and $\nu(CO_{amide})$ bands at ~1740 and ~1660 cm^{-1} (see Figure 2A and Figure 3 vs. Figure 4 left). Further, in Figure 2A and Figure 3A we noted that SEIRA spectra in presence of Na^+ showed redshifts of ester and amide bands by ~−1 and ~−7 cm^{-1}, respectively, when compared to K^+ and washing with fresh buffer led to an additional change observed in amide range (Figure 2A, difference spectrum in grey). Satisfying both observations, we can propose the distorted $EB_2:Na^+$ complex at/in the membrane as a main species (red peaks in Figure 3B and spectra Figure 4), which coexists with an additional fraction of $EB:Na^+_{out}$, (blue peaks in Figure 3B and spectra Figure 4). This interpretation explains the broader band shape in comparison to the spectra in K^+. In Figure S5, we show that a 2:1 mixture of the DFT-IR-spectra of the distorted $EB_2:Na^+$ and $EB:Na^+_{out}$ can satisfactorily reproduce the SEIRA spectra and the differences with respect to spectra in K^+.

In the case of Cs^+ we detect similar peak shifts of ester and amide bands by ~−1 and ~−6 cm^{-1}, respectively, when compared to K^+. Modelling this situation using our DFT-predicted spectra requires a mixture of $EB_2:Cs^+$ and $EB:Cs^+_{out}$ (red and blue peaks/spectra, respectively, in Figure 3B and 4; see Figure S5). By contrast, the pure species would predict negligible (−1 and −1 cm^{-1}) or too large changes (+1 and −12 cm^{-1}), respectively, with respect to spectra with K^+, contrary to our SEIRA spectra. Figure S5 shows spectra according to this interpretation (in a 1:2 mixture), again providing a satisfactory match to experimental spectra observed in Figure 2A and 3A.

As obvious from SEIRA spectra with Li^+, Mg^{2+}, and Ca^{2+} also here mixtures of species can be proposed, even though the assignment is aggravated by the broad spectral features. However, the observation of several bands in the $\nu(CO_{ester})$

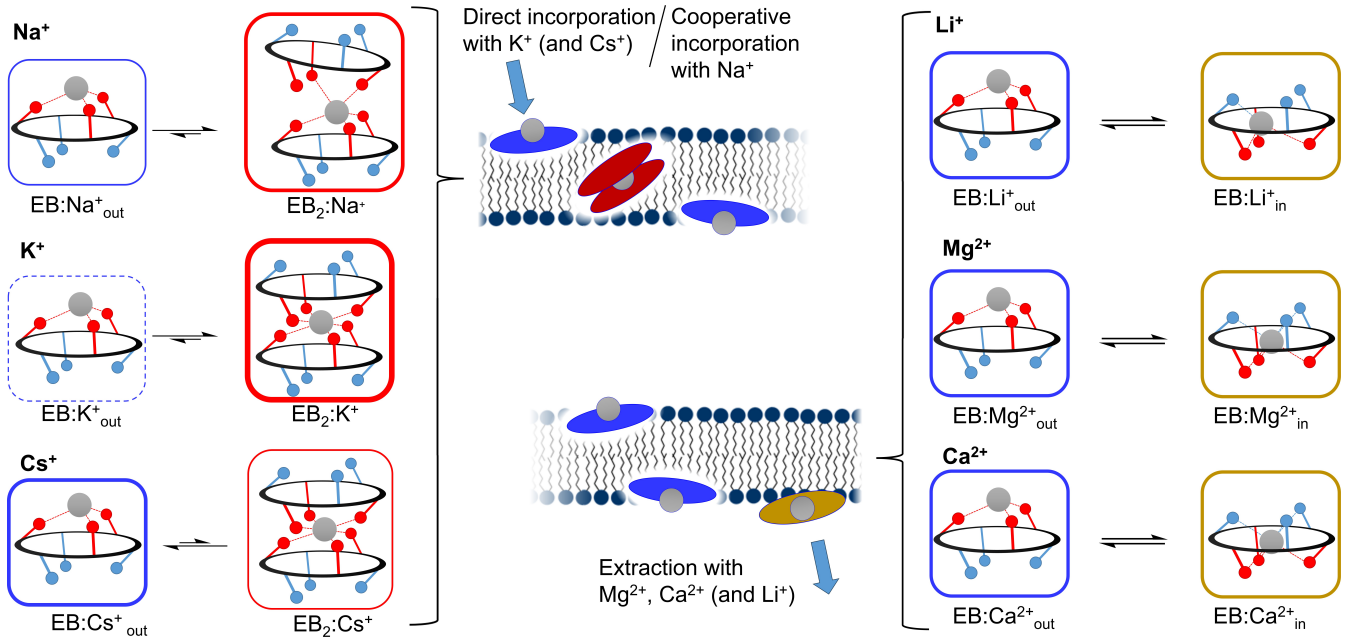

Figure 5. Membrane-associated $EB_n:M^{z+}$ complexes suggested by the combination of experimental SEIRA and DFT-computed spectra, and implications for incorporation and membrane interactions. **Left**: Na^+, K^+, and Cs^+ form open-faced $EB:M^+$ (blue frame) and $EB_2:M^+$ sandwich (red frame) complexes; the latter is asymmetric in the case of Na^+. The strength of the frame and the equilibrium indicate the predominant species. **Right:** Li^+, Mg^{2+}, and Ca^{2+} form predominantly open-faced $EB:M^{1/2+}$ (blue frame) and belted $EB:M^{1/2+}$ (yellow frame) complexes. **Middle**: EB incorporates into the membrane in the presence of Na^+, K^+, and Cs^+, and can exchange these ions as a membrane-associated species. Instead, the presence of Li^+, Mg^{2+}, and Ca^{2+} is associated with (partial) removal of EB from the membrane. Note that EB complexes may adopt a range of orientation and not only the ones shown as examples in this figure.

range and the feature at ~1560–1550 cm^{-1} in Mg^{2+} and Ca^{2+}, which can be assigned to the ligating amide C=O groups, indicates the presence of either $EB:M^{z+}_{in}$ or $EB:M^{z+}_{out}$ structures and absence of $EB_2:M^{z+}$ (see summary in Figure 5). This assertion is supported for Mg^{2+} and Ca^{2+} by the clear separation of the $\nu(CO_{amide})$ ~1560–1550 cm^{-1} and the bands >1600 cm^{-1} in SEIRA spectra, in between which the $\nu(CO_{amide})$ of $EB_2:M^{z+}$ would be observed according to DFT-based IR spectra (i.e. red peak at ~1610 cm^{-1} between yellow and blue feature in Figure 4). For Li^+, this assignment is solely based on the low probability of the highly asymmetric $EB_2:Li^+$ in solution phase, where the singly-ligating EB ring is expected to dissociate easily.

Implications of the Assignments for the Molecular Mechanism of EB Incorporation Into Membranes

Based on the assignments in the previous section and the observed complexes formed with specific cations according to DFT calculations, it is now interesting to elaborate on the difference of the observed kinetics in presence of Na^+ and K^+ in terms of a molecular picture. Here, we want to remind that EB did not incorporate noticeably into the membrane in the absence of ions (as judged by SEIRA spectra in Figure S3).

In general, for the spontaneous incorporation process associated with the apparent rate constant k_{spon}, it can be expected that the better the charge of the cation is screened by EB molecules, the lower the activation barrier for the incorporation into the membrane core will be. Among the possible structures, the 2:1 sandwich complex provides the highest degree of charge screening being surrounded by a 5–7 Å organic layer created by two EB molecules. Since EB and K^+ adopt such a $EB_2:K^+$ complex according to our and previous assignments (as it is the case for Cs^+), it is not surprising that the spontaneous incorporation occurs efficiently on the similar time scales as observed previously for peptides forming transmembrane channels.[32,33] In this light, it is therefore also comprehensible that in presence of Na^+ this process is hindered, since a uniform 2:1 sandwich complex cannot be formed according to DFT results. Accordingly, our data excludes the presence of belted 1:1 $EB:Na^+_{in}$ complex, and points to the predominant presence of the distorted $EB_2:Na^+$ and the $EB:Na^+_{out}$ as main membrane-associated structures. Since both structures will screen the ion's charge less efficiently than an "ideal" $EB_2:M^+$ complex, direct incorporation will be hindered, and thus the considerable difference in activation barrier is observed. Importantly, despite its asymmetric structure, only the distorted $EB_2:Na^+$ would provide sufficient charge screening to incorporate into the hydrophobic membrane interior.

The autocatalytic process observed in presence of Na^+ is much more difficult to rationalize in detail based on the present data, since components beyond the detection limit of SEIRA can likely contribute to the mechanism. However, one can assume that the distorted 2:1 $EB_2:Na^+$ can again play an important role in the positively cooperative incorporation behaviour (modelled using an *autocatalytic* kinetic scheme) as a the main species within the membrane core. Accordingly, one

EB ligand of the distorted 2:1 EB_2:Na^+ sandwich structure will lack the stabilizing benefits of the kinetic chelate effect of the 3-coordinating EB. As such, EB molecules can get more easily abstracted due to an increased number of H-bond interactions with molecules in the head group region or due to the presence of EB:Na^+_{out} complexes. This potential quick exchange and, thus, transient spectroscopically non-detectable species (such as free EB) could act as a mediator for incorporation. In this context, it is interesting to note that it was demonstrated previously that Na^+ ions but not K^+ ions reside deeply within the lipid head group region.[68,69] As a consequence, the local K^+ concentrations sensed by membrane-bound EB molecules is considerably lowered, such that the specific behaviour of EB in presence of Na^+ may play an important role for membrane incorporation.

Further Implications for EB's Activity

Enniatins have been reported to show specific enzyme inhibiting and mitochondriotoxic properties, which are relevant to their anticancer activity as well as to potential human and animal health issues.[3] A prerequisite for such functions of enniatins is the entry into the cell such that the specific targets can be reached. Na^+ and K^+ are main cations in the extracellular medium and our experiments support that their presence assists the incorporation into the membrane (Figure 2 and summary in Figure 5). Ion exchange experiments using the mono-valent Na^+, K^+ and Cs^+ allowed detecting the proposed EB_n:M^+ species, which were adopted reversibly (Figure 3, Figure S4), suggesting this as a common behavior of EB with alkaline cations (except for Li^+). Instead, we note that Li^+, Mg^{2+}, and Ca^{2+} demonstrated irreversible behavior, in which EB was extracted from the membrane judging by the overall SEIRA intensities (Figure 3, Figure S4). As such, overall bivalent cations could play a relevant role of abstracting EB from the membrane and thus facilitating the transfer into the intracellular medium. The observation that Li^+ stands as the exception to these assertions can be rationalized based on the diagonal relationship between Li^+ and Mg^{2+} due their similar charge densities of 100–120 C mm^{-3}. Despite the much lower physiological concentrations of Mg^{2+} and Ca^{2+} it is again noteworthy that both ions (together with Na^+ and Li^+, but not K^+) are enriched within the membrane headgroup region,[68,69] providing direct access to efficiently bind EB. If membrane extraction is mediated by EB complexes with Mg^{2+} and Ca^{2+} (and Li^+), the belted 1:1 EB:M^{z+}_{in} complex is a likely candidate in this process as it provide a minimal charge screening for the cations.

Recently, Su et al.[58,59] used a combination of supported membranes and infrared spectroscopy to study the ionophoric mechanism of valinomycin, which enniatins are frequently compared to. Valinomycin is a K^+-selective dodecadepsipeptide (K^+:Na^+-selectivity ratio of 100 000:1)[70] containing 12 C=O groups as potential ligands for the complexation of cations. The studies[58,59] showed that the anion can modulate the K^+-transport via additional ion-pairing with the cation-complex. In our study, we only used Cl^- as counter ion to avoid compounding our data with such additional effects. However, similar counter-ion-based influences can be imagined for EB_2:K^+-complexes, and could be even more pronounced for complexes with other cations with a lower degree of charge screening. This may not only affect the cation transport, but also the incorporation and extraction mechanism proposed in Figure 5.

Conclusions

Enniatins are promising antimicrobial and anticancer agents based on their ionophoric, enzyme inhibiting and mitochondriotoxic properties.[3] Using the combination of SEIRA spectroscopy and tBLMs assisted by DFT-based computational spectroscopy, we have characterized the cation-dependent behaviour of EB_n:M^{z+}-complexes modulating the incorporation and interaction with the lipid membrane, in which they can act as ionophores. Overall, we find (as summarized in Figure 5)

- that the monovalent K^+ and Na^+ promote EB-membrane incorporation with distinctly different kinetics. In presence of K^+, a direct incorporation is observed, which we associate with the a dominating 2:1 EB_2:K^+ sandwich structure.
- Instead in presence of Na^+, a sigmoidal shaped kinetics of incorporation occurs. This can be rationalized in terms of an positively cooperative/*autocatalytic* process that is mediated via a mixture of distorted 2:1 EB_2:Na^+ sandwich structures and 1:1 open-faced EB:Na^+_{out} complexes.
- In contrast to monovalent ions like Na^+, K^+, and Cs^+, the bivalent Mg^{2+} and Ca^{2+} (and the similarly high-charge-density Li^+) ions removed EB from the membrane, indicating a potential role for the transition of EB into the intracellular medium. One factor contributing to this behaviour may be the adoption of the belted 1:1 EB:M^{z+}_{in} complexes, which provide a small degree of charge screening.

As enniatins can be conveniently derivatized using the concepts such as hybrid modular non-ribosomal peptide synthetases to tune their bioactivity,[16] physicochemical platforms that combine molecular spectroscopy with bilayer lipid membranes,[34,36,71–73] as the one presented in this work, are important tools to provide rationale to their molecular mechanisms of action.

Supporting Information

Further data can be found in the supporting information: SEIRA and impedance spectra of tBLM assembly; water background correction; EB incorporation SEIRA spectra with Na^+, K^+, Cs^+ and without cations; Cation dependent reversibility in SEIRA spectra of EB; Kinetic model for EB membrane incorporation; SEIRA spectra during ion exchange. Additional literature has been cited in the supporting information.[74,75]

Acknowledgements

B.D.G. acknowledges the School for Analytical Sciences Adlershof (SALSA) for PhD fellowship. G.Y. thanks the Alexander von Humboldt-Stiftung for a Humboldt research fellowship. The authors thank Dr. Lennart Richter and Prof. Dr. Roderich Süßmuth (Technische Universität Berlin, Institute of Chemistry, Biological Chemistry) for providing enniatin B for this work. P.K. acknowledges Transdisciplinary Research Area 'Building Block of Matter and Fundamental Interactions', University of Bonn. J.K. thanks the HPC Service of ZEDAT, Freie Universität Berlin, for computing time (10.17169/refubium-26754). The authors thank the Deutsche Forschungsgemeinschaft (DFG; German Research Foundation) for financial support via EXC-2008-390540038-"UniSysCat" (M.A.M. and P.H.) and the Sonderforschungsbereich 1078 "Protonation Dynamics in Protein Function" (project number 221545957-project B09, J.K.). Open Access funding enabled and organized by Projekt DEAL.

Conflict of Interests

The authors declare no conflict of interest.

Data Availability Statement

Optimized structures of enniatin B:cation complexes are available under https://github.com/KozuchLab/Publications/tree/main/Enniatin_DFT. Further data that support the findings of this study are available from the corresponding author upon reasonable request.

Keywords: enniatin · bilayer lipid membrane · surface-enhanced infrared absorption · ionophore · anticancer

[1] R. Süssmuth, J. Müller, H. von Döhren, I. Molnár, *Nat. Prod. Rep.* **2011**, *28*, 99–124.
[2] T. Dang, R. D. Süssmuth, *Acc. Chem. Res.* **2017**, *50*, 1566–1576.
[3] A. Prosperini, H. Berrada, M. J. Ruiz, F. Caloni, T. Coccini, L. J. Spicer, M. C. Perego, A. Lafranconi, *Front. Public Heal.* **2017**, *5*, 304.
[4] M. Jestoi, *Crit. Rev. Food Sci. Nutr.* **2008**, *48*, 21–49.
[5] S. Uhlig, M. Jestoi, P. Parikka, *Int. J. Food Microbiol.* **2007**, *119*, 17–24.
[6] M. de Nijs, H. van den Top, J. de Stoppelaar, P. Lopez, H. Mol, *Food Chem.* **2016**, *213*, 763–767.
[7] C. K. Fæste, L. Ivanova, S. Uhlig, *Drug Metab. Dispos.* **2011**, *39*, 1768–76.
[8] F. Tedjiotsop Feudjio, R. Dornetshuber, M. Lemmens, O. Hoffmann, R. Lemmens-Gruber, W. Berger, *World Mycotoxin J.* **2010**, *3*, 415–430.
[9] R. Dornetshuber-Fleiss, D. Heilos, T. Mohr, L. Richter, R. D. Süssmuth, M. Zlesak, A. Novicky, P. Heffeter, R. Lemmens-Gruber, W. Berger, *Biochem. Pharmacol.* **2015**, *93*, 318–331.
[10] R. Dornetshuber, P. Heffeter, M. Sulyok, R. Schumacher, P. Chiba, S. Kopp, G. Koellensperger, M. Micksche, R. Lemmens-Gruber, W. Berger, *Mol. Nutr. Food Res.* **2009**, *53*, 904–920.
[11] R. Dornetshuber, P. Heffeter, R. Lemmens-Gruber, L. Elbling, D. Marko, M. Micksche, W. Berger, *Mol. Nutr. Food Res.* **2009**, *53*, 1112–1122.
[12] R. Dornetshuber, P. Heffeter, M.-R. Kamyar, T. Peterbauer, W. Berger, R. Lemmens-Gruber, *Chem. Res. Toxicol.* **2007**, *20*, 465–473.
[13] W. Wätjen, A. Debbab, A. Hohlfeld, Y. Chovolou, A. Kampkötter, R. A. Edrada, R. Ebel, A. Hakiki, M. Mosaddak, F. Totzke, M. H. G. Kubbutat, P. Proksch, *Mol. Nutr. Food Res.* **2009**, *53*, 431–440.
[14] Y. A. Ovchinnikov, V. T. Ivanov, A. V. Evstratov, I. I. Mikhaleva, V. F. Bystrov, S. L. Portnova, T. A. Balashova, E. N. Meshcheryakova, V. M. Tulchinsky, *Int. J. Pept. Protein Res.* **1974**, 465–498.
[15] M. Kamyar, P. Rawnduzi, C. R. Studenik, K. Kouri, R. Lemmens-Gruber, *Arch. Biochem. Biophys.* **2004**, *429*, 215–23.
[16] S. Zobel, S. Boecker, D. Kulke, D. Heimbach, V. Meyer, R. D. Süssmuth, *ChemBioChem* **2016**, *17*, 283–287.
[17] S. Lifson, C. E. Felder, A. Shanzer, *J. Biomol. Struct. Dyn.* **1984**, *2*, 641–661.
[18] R. Benz, *J. Membr. Biol.* **1978**, *43*, 367–394.
[19] Y. A. Ovchinnikov, *FEBS Lett.* **1974**, *44*, 1–21.
[20] V. T. Ivanov, A. V. Evstratov, L. V. Sumskaya, E. I. Melnik, T. S. Chumburidze, S. L. Portnova, T. A. Balashova, Y. A. Ovchinnikov, *FEBS Lett.* **1973**, *36*, 65–71.
[21] N. E. Zhukhlistova, *Crystallogr. Reports* **2002**, *47*, 433–442.
[22] S. Rebaud, O. Maniti, A. P. Girard-Egrot, *Biochimie* **2014**, *107*, 135–142.
[23] J. Kozuch, K. Ataka, J. Heberle, *Nat. Rev. Methods Prim.* **2023**, *3*, 70.
[24] J. Kozuch, C. Weichbrodt, D. Millo, K. Giller, S. Becker, P. Hildebrandt, C. Steinem, *Phys. Chem. Chem. Phys.* **2014**, *16*, 9546–9555.
[25] S. Wiebalck, J. Kozuch, E. Forbrig, C. C. Tzschucke, L. J. C. C. Jeuken, P. Hildebrandt, *J. Phys. Chem. B* **2016**, *129*, 2249–2256.
[26] O. Gutiérrez-Sanz, E. Forbrig, A. P. Batista, M. M. Pereira, J. Salewski, M. A. Mroginski, R. Götz, A. L. De Lacey, J. Kozuch, I. Zebger, *Langmuir* **2018**, *34*, 5703–5711.
[27] R. Paschke, S. Mohr, S. Lange, A. Lange, J. Kozuch, *Angew. Chem. Int. Ed.* **2023**, *62*, e20230906.
[28] S. Kriegel, T. Uchida, M. Osawa, T. Friedrich, P. Hellwig, *Biochemistry* **2014**, *53*, 6340–6347.
[29] X. Jiang, E. Zaitseva, M. Schmidt, F. Siebert, M. Engelhard, R. Schlesinger, K. Ataka, R. Vogel, J. Heberle, *Proc. Natl. Acad. Sci. USA* **2008**, *105*, 12113–12117.
[30] K. Ataka, F. Giess, W. Knoll, R. L. C. Naumann, S. Haber-Pohlmeier, B. Richter, J. Heberle, *J. Am. Chem. Soc.* **2004**, *126*, 16199–206.
[31] E. Zaitseva, M. Saavedra, S. Banerjee, T. P. Sakmar, R. Vogel, *Biophys. J.* **2010**, *99*, 2327–2335.
[32] J. Kozuch, C. Steinem, P. Hildebrandt, D. Millo, *Angew. Chem. Int. Ed.* **2012**, *51*, 8114–8117.
[33] E. Forbrig, J. K. J. K. Staffa, J. Salewski, M. A. Mroginski, P. Hildebrandt, J. Kozuch, *Langmuir* **2018**, *34*, 2373–2385.
[34] A. de Miguel Catalina, E. Forbrig, J. Kozuch, C. Nehls, L. Paulowski, T. Gutsmann, P. Hildebrandt, M.-A. Mroginski, *Biochemistry* **2019**, *58*, 2447–2462.
[35] M. A. Fallah, C. Stanglmair, C. Pacholski, K. Hauser, *Langmuir* **2016**, *32*, 7356–7364.
[36] K. Ataka, J. Drauschke, V. Stulberg, B. Koksch, J. Heberle, *Biochim. Biophys. Acta Biomembr.* **2022**, *1864*, 183873.
[37] P. Kielb, M. Sezer, S. Katz, F. Lopez, C. Schulz, L. Gorton, R. Ludwig, U. Wollenberger, I. Zebger, I. M. Weidinger, *ChemPhysChem* **2015**, *16*, 1960–1968.
[38] C. Steiniger, S. Hoffmann, A. Mainz, M. Kaiser, K. Voigt, V. Meyer, R. D. Süssmuth, *Chem. Sci.* **2017**, *8*, 7834–7843.
[39] H. Miyake, S. Ye, M. Osawa, *Electrochem. Commun.* **2002**, *4*, 973–977.
[40] J. K. R. Kendall, B. R. G. Johnson, P. H. Symonds, G. Imperato, R. J. Bushby, J. D. Gwyer, C. van Berkel, S. D. Evans, L. J. C. Jeuken, *ChemPhysChem* **2010**, *11*, 2191–2198.
[41] L. J. C. Jeuken, N. N. Daskalakis, X. Han, K. Sheikh, A. Erbe, R. J. Bushby, S. D. Evans, *Sens. Actuators B* **2007**, *124*, 501–509.
[42] E. K. Schmitt, M. Nurnabi, R. J. Bushby, C. Steinem, *Soft Matter* **2008**, *4*, 250–253.
[43] A. D. Becke, *Phys. Rev. A* **1988**, *38*, 3098–3100.
[44] J. P. Perdew, *Phys. Rev. B* **1986**, *33*, 8822–8824.
[45] M. J. Frisch, G. W. Trucks, H. B. Schlegel, G. E. Scuseria, M. A. Robb, J. R. Cheeseman, G. Scalmani, V. Barone, B. Mennucci, G. A. Petersson, H. Nakatsuji, M. Caricato, X. Li, H. P. Hratchian, A. F. Izmaylov, J. Bloino, G. Zheng, J. L. Sonnenberg, M. Hada, M. Ehara, K. Toyota, R. Fukuda, J. Hasegawa, M. Ishida, T. Nakajima, Y. Honda, O. Kitao, H. Nakai, T. Vreven, J. Montgomery, J. A., J. E. Peralta, F. Ogliaro, M. Bearpark, J. J. Heyd, E. Brothers, K. N. Kudin, V. N. Staroverov, R. Kobayashi, J. Normand, K. Raghavachari, A. Rendell, J. C. Burant, S. S. Iyengar, J. Tomasi, M. Cossi, N. Rega, J. M. Millam, M. Klene, J. E. Knox, J. B. Cross, V. Bakken, C. Adamo, J. Jaramillo, R. Gomperts, R. E. Stratmann, O. Yazyev, A. J. Austin, R. Cammi, C. Pomelli, J. W. Ochterski, R. L. Martin, K. Morokuma, V. G. Zakrzewski, G. A. Voth, P. Salvador, J. J. Dannenberg, S. Dapprich, A. D. Daniels, Ö. Farkas, J. B. Foresman, J. V. Ortiz, J. Cioslowski, D. J. Fox, **2016**.

[46] N. Elghobashi-Meinhardt, D. Tombolelli, M. A. Mroginski, *Catalysts* **2021**, *11*, 245.
[47] A. Boda, M. A. Sheikh, *J. Phys. Chem. A* **2012**, *116*, 8615–8623.
[48] W. J. Hehre, R. Ditchfield, J. A. Pople, *J. Chem. Phys.* **1972**, *56*, 2257–2261.
[49] F. Weigend, R. Ahlrichs, *Phys. Chem. Chem. Phys.* **2005**, *7*, 3297–3305.
[50] T. Leininger, A. Nicklass, W. Küchle, H. Stoll, M. Dolg, A. Bergner, *Chem. Phys. Lett.* **1996**, *255*, 274–280.
[51] J. Tomasi, B. Mennucci, R. Cammi, *Chem. Rev.* **2005**, *105*, 2999–3093.
[52] C. R. Groom, I. J. Bruno, M. P. Lightfoot, S. C. Ward, *Acta Crystallogr.* **2016**, *72*, 171–179.
[53] M. Dobler, J. D. Dunitz, J. Krajewski, *J. Mol. Biol.* **1969**, *42*, 605–606.
[54] A. V. Melkikh, M. I. Sutormina, *J. Theor. Biol.* **2008**, *252*, 247–254.
[55] F. Siebert, P. Hildebrandt, *Vibrational Spectroscopy in Life Science*, WILEY-VCH Verlag GmbH & Co. KGaA, Weinheim, **2008**.
[56] A. Barth, *Biochim. Biophys. Acta* **2007**, *1767*, 1073–1101.
[57] A. M. Bapolisi, P. Kielb, M. Bekir, A. C. Lehnen, C. Radon, S. Laroque, P. Wendler, H. M. Müller-Werkmeister, M. Hartlieb, *Macromol. Rapid Commun.* **2022**, *43*, 2200288.
[58] Z. F. Su, X. Q. Ran, J. J. Leitch, A. L. Schwan, R. Faragher, J. Lipkowski, *Langmuir* **2019**, *35*, 16935–16943.
[59] Z. Su, J. J. Leitch, S. Sek, J. Lipkowski, *Langmuir* **2021**, *37*, 9613–9621.
[60] S. H. Schneider, S. G. Boxer, *J. Phys. Chem. B* **2016**, *120*, 9672–9684.
[61] J. Kozuch, S. Schneider, C. Zheng, Z. Ji, R. T. Bradshaw, S. Boxer, *J. Phys. Chem. B* **2021**, *125*, 4415–4427.
[62] S. D. Fried, S. G. Boxer, *Acc. Chem. Res.* **2015**, *48*, 998–1006.
[63] Q. Cui, M. Karplus, *Protein Sci.* **2008**, *17*, 1295–1307.
[64] V. J. Hilser, J. O. Wrabl, H. N. Motlagh, *Annu. Rev. Biophys.* **2012**, *41*, 585–609.
[65] S. Liu, *J. Colloid Interface Sci.* **2015**, *450*, 224–238.
[66] E. G. Prout, F. C. Tompkins, *Trans. Faraday Soc.* **1944**, *40*, 488.
[67] M. E. Brown, *Thermochim. Acta* **1997**, *300*, 93–106.
[68] A. Cordomí, O. Edholm, J. J. Perez, *J. Phys. Chem. B* **2008**, *112*, 1397–408.
[69] B. Klasczyk, V. Knecht, R. Lipowsky, R. Dimova, *Langmuir* **2010**, *26*, 18951–8.
[70] M. C. Rose, R. W. Henkens, *Biochim. Biophys. Acta Gen. Subj.* **1974**, *372*, 426–435.
[71] M. A. Fallah, K. Hauser, *Biomater. Sci.* **2019**, *7*, 3204–3212.
[72] Z. Su, J. J. Leitch, J. Lipkowski, *Curr. Opin. Electrochem.* **2018**, In Press.
[73] I. Brand, B. Khairalla, *Faraday Discuss.* **2021**, *232*, 68–85.
[74] F. H. Pilz, P. Kielb, *BBA Adv.* **2023**, *4*, 100095.
[75] Z. Su, J. Juhaniewicz-Debinska, S. Sek, J. Lipkowski, *Langmuir* **2020**, *36*, 409–418.

Manuscript received: February 28, 2024
Revised manuscript received: April 26, 2024
Accepted manuscript online: May 3, 2024
Version of record online: May 22, 2024